Hindawi
Geofluids
Volume 2022, Article ID 9610289, 16 pages
https://doi.org/10.1155/2022/9610289

Research Article

Stability Analysis of Shield Inclined Tunnel Faces under the Change Effect of Soil Heterogeneity and Pore Water with Buried Depth

Hong Sun,[1] Dao-bing Zhang,[1,2] Hua-dong Yin ,[2] and A-ping Hu[2]

[1]*School of Civil Engineering, Hunan University of Science and Technology, Xiangtan 411201, China*
[2]*School of Resource Environment and Safety Engineering, Hunan University of Science and Technology, Xiangtan 411201, China*

Correspondence should be addressed to Hua-dong Yin; 21300102001@mail.hnust.edu.cn

Received 31 March 2022; Accepted 24 May 2022; Published 7 July 2022

Academic Editor: Xinyu Ye

The purpose of this work is to look at how soil heterogeneity and pore water pressure impact shield inclined tunnel excavation face stability as burial depth varies. The calculation model of excavation face stability was established, and the supporting pressure of maintain the excavation face stability was solved via the upper bound method. The results showed that the soil heterogeneity coefficient and pore water pressure coefficient had substantial effects on the supporting pressure. The location of failure face and failure range of shield inclined tunnel under varied heterogeneity coefficient and pore water pressure coefficient were presented. In addition, the boundary depth of shallow tunnel under the influence of soil heterogeneity and pore water was obtained, which supplemented the relevant tunnel code.

1. Introduction

The shield method is widely applied in subway and tunnel construction as its benefits of safe excavation and fast driving speed. Due to the complex geological conditions, the construction requirements are relatively high, and the surface settlement is required to be controlled within the millimeter range, so it is very important to set a reasonable thrust (support pressure) to ensure the shield tunneling smoothly. Some scholars believe that most rocks and soils in nature have heterogeneity [1–3]. For shield inclined tunnels, the soil heterogeneity and pore water effect also change with the buried depth constantly changing, which seriously affects the stability of the shield tunnels. Therefore, it is statistically significant to research the stability of shield inclined tunnels under soil heterogeneity and pore water pressure effect. The key to solve this problem is to determine the reasonable support pressure under different buried depths, which has significant scientific research value and engineering significance [4–8].

For geotechnical engineering, especially tunnel engineering stability analysis, the limit analysis upper bound method has been an excellent theoretical analysis method [9–14]. Ibrahim et al. [15] established the failure mode of tunnel excavation face by "point-to-point" method for tunnels in layered soil. The representation of the support resistance of excavation face in layered soil was deduced via the virtual power principle in limit analysis method, and the upper limit solution of the support resistance was solved. Han et al. [16] analyzed the mechanical state of the multilayer soil and constructed the multiblock failure mode of the tunnel excavation face. The upper limit solution of the supporting pressure in the situation of multilayered soil was solved by the limit analysis upper bound method. It was compared to previous findings, and the accuracy of the computation procedure was confirmed. Pan and Dias [17] established the noncircular tunnel failure mechanism working face via the limit analysis method and the strength reduction method. The security factor of excavation face was estimated, and the influence of different section shapes on the safety factor was discussed. Senent et al. [18] constructed a failure mechanism including translational and rotational motions through limit analysis theory. The collapse pressure of tunnel face considering free span was calculated, and the

logic of mechanism was confirmed using numerical simulation. None of the above studies explored the pore water effect. After realizing the importance of pore water effect, some scholars also carried out research. Chen et al. [19] considered the pore water pressure effect on the critical supporting pressure of tunnel face and proposed a method to calculate it via the upper bound theorem. Finite element analysis was used to verify the validity of the suggested technique. Li et al. [20] considered the pore water effect of deep buried tunnel and used nonlinear limit analysis upper limit theorem to construct a three-dimensional collapse failure mode of deep-buried tunnels, deduced the calculation formula for the three-dimensional collapse failure range, which provides theoretical guidance for deep buried tunnel optimization design. Xu et al. [21] proposed a combined translational and rotational failure mode in the stability analysis of the tunnel excavation face. The pore water effect into calculation model was introduced. The limit analysis upper bound method is used to solve the excavation face supporting pressure and the potential failure surface under the pore water effect.

The above studies assume that the buried depth of the tunnel remains unchanged; that is, the research results are applicable to noninclined tunnels. To the shield inclined tunnels, the buried depth is constantly changing, and the shield tunnel stability is affected by the soil heterogeneity and pore water pressure effect to varying degrees. The soil heterogeneity and the effect of pore water were considered via the existing research results in this work, and the limit analysis upper bound method was adopted to calculate the supporting pressure necessary for shield inclined tunnels excavation surface stability.

2. Upper Bound Theorem of Limit Analysis considering the Pore Pressure Effect

The pore water is a vital factor leading to instability of geotechnical engineering. For the problem of tunnel stability under the pore water effect, the pore water pressure was included as an external factor in the upper limit analysis method by several scholars [22–24]. The upper limit analysis theorem of pore pressure effect was established. In this theory, the pore water pressure was regarded as external force acting on the soil particles, and the power generated by the pore water pressure was divided into two parts. One is that the pore water pressure causes volume strain in the soil, and the other is the pore water pressure effect on the velocity interruption surface. Its expression is as follows:

$$\int_V \sigma_{ij}\dot{\varepsilon}_{ij}\mathrm{d}V \geq \int_S T_i v_i dS + \int_V F_i v_i \mathrm{d}V - \int_V u\dot{\varepsilon}_{ij} dV + \int_S u n_i v_i dS, \tag{1}$$

where σ_{ij} and $\dot{\varepsilon}_{ij}$, respectively, are the stress tensor and strain rate at any point in the plastic failure zone; V and F_i are the microvolume and volume force in the plastic failure zone, respectively; T_i is the surface force acting on the boundary S in the plastic failure zone; v_i is the velocity on the discontinuous line of velocity; u is the pore water pressure; and n_i is the discontinuity face normal direction.

3. Calculation Model

A calculation model of excavation face stability of shield inclined tunnels considering soil heterogeneity and pore water pressure effect was established by the existing literature [25–28] in this work. Figure 1 depicts the inclined tunnel excavation facing AB, M is the excavation face midpoint, the tunnel diameter and buried depth are, respectively, d and h, and the tunnel inclination angle is α. When the excavation face is failure, it spins at an angular velocity ω around point O, and the body destruction is AEB. The inner and outer boundaries of the body destruction AEB are logarithmic spirals AE and BE, and their expressions are $r_1(\theta) = r_a \exp[(\theta - \theta_2)\tan\varphi]$, $r_2(\theta) = r_b \exp[(\theta_1 - \theta)\tan\varphi]$. The angle of vertex E is 2φ, and φ is the internal friction angle of soil. r_a and r_b are the lengths of OA and OB, respectively, and θ_1, θ_2, and θ_3 are the angles between the vertical direction and OB, OA, and OE, respectively. Meanwhile, u is the pore water pressure, γ is the volumetric weight of soil, and σ_T is the uniform supporting pressure on the excavation face.

The soil cohesion c varies linearly with depth, and then [29, 30]:

$$c = c_0 + \rho(h - z), \tag{2}$$

where c_0 is the initial cohesion of the soil, ρ is the coefficient of soil heterogeneity, reflecting the relationship of cohesion with depth, and z is the distance from a certain point in the soil to the ground surface.

4. Upper Bound Solution

4.1. Soil Weight Power. In Figure 1, the failure area ABE can be separated into the upper area AEB' and the bottom area ABB'. Under the action of the soil weight, the power generated in area AEB' is $W_{\gamma\text{-AEB}'}$, and in it, the area ABB' is $W_{\gamma\text{-ABB}'}$, and the expressions are as follows:

$$W_{\gamma\text{-AEB}'} = \gamma \cdot \omega \cdot r_b^3 \cdot \left[g_1 - \frac{\sin^3(\theta_1 + \alpha)}{\sin^3(\theta_2 - \theta_1)} g_2 \right], \tag{3}$$

$$W_{\gamma\text{-ABB}'} = \gamma \cdot \omega \cdot r_b^3 \cdot g_3, \tag{4}$$

where $g_1 \sim g_3$ are, respectively:

$$\begin{aligned} g_1 &= \frac{1}{3}\int_{\theta_2}^{\theta_3} e^{[3(\theta_1-\theta)\cdot\tan\varphi]} \cdot \sin\theta d\theta \\ &= \frac{\tan\varphi \cdot \left\{ \sin\theta_2 \cdot e^{[3(\theta_1-\theta_2)\cdot\tan\varphi]} - \sin\theta_3 e^{[3(\theta_1-\theta_3)\cdot\tan\varphi]} \right\}}{(1 + 9\tan^2\varphi)} \\ &\quad + \frac{\cos\theta_2 e^{[3(\theta_1-\theta_2)\cdot\tan\varphi]} - \cos\theta_3 \cdot e^{[3(\theta_1-\theta_3)\cdot\tan\varphi]}}{3(1 + 9\tan^2\varphi)}, \end{aligned} \tag{5}$$

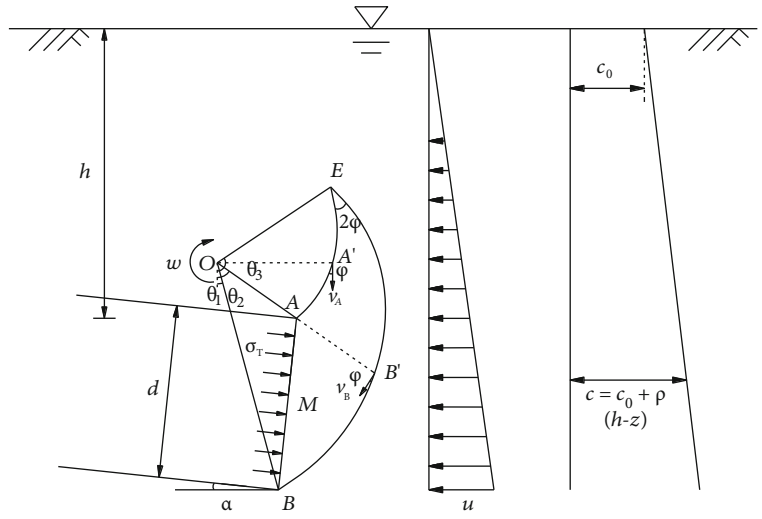

Figure 1: Calculation model for stability of excavation face of shield inclined tunnel.

$$g_2 = \frac{1}{3}\int_{\theta_2}^{\theta_3} e^{[3(\theta-\theta_2)\cdot\tan\varphi]}\cdot\sin\theta d\theta = \frac{\tan\varphi\cdot\left\{\sin\theta_3\cdot e^{[3(\theta_3-\theta_2)\cdot\tan\varphi]}-\sin\theta_2\right\}}{(1+9\tan^2\varphi)} + \frac{\cos\theta_2-\cos\theta_3\cdot e^{[3(\theta_3-\theta_2)\cdot\tan\varphi]}}{3(1+9\tan^2\varphi)}, \tag{6}$$

$$g_3 = \frac{1}{3}\left\{\int_{\theta_1}^{\theta_2} e^{[3(\theta_1-\theta)\cdot\tan\varphi]}\cdot\sin\theta d\theta - \frac{\sin(\theta_2-\theta_1)\sin^2\theta_1}{\sin(\theta_2+\alpha)}\right\} = \frac{\tan\varphi\left\{\sin\theta_1-\sin\theta_2\cdot e^{[3(\theta_1-\theta_2)\cdot\tan\varphi]}\right\}}{(1+9\tan^2\varphi)} + \frac{1}{3}\left\{\frac{\cos\theta_1-\cos\theta_2\cdot e^{[3(\theta_1-\theta_2)\cdot\tan\varphi]}}{(1+9\tan^2\varphi)} + \frac{\sin(\theta_2-\theta_1)\sin^2\theta_1}{\sin(\theta_2+\alpha)}\right\}. \tag{7}$$

Then, the total soil weight power of ABE in the failure area is:

$$W_\gamma = W_{\gamma\text{-AEB}'} + W_{\gamma\text{-ABB}'}. \tag{8}$$

4.2. Supporting Pressure Power. The power of the support force σ_T in the failure area AEB is the sum of the product of the support force σT and the tunnel face velocity:

$$W_T = \int_{\theta_1}^{\theta_2}\frac{r_b}{\sin(\theta+\alpha)}\cdot\sin(\theta_1+\alpha)\cdot\omega\cdot\cos(\theta+\alpha)\cdot\sigma_T \cdot\frac{r_b}{\sin^2(\theta+\alpha)}\cdot\sin(\theta_1+\alpha)d\theta = \frac{1}{2}\sigma_T\cdot\omega\cdot r_b^2 \cdot\left[1-\frac{\sin^2(\theta_1+\alpha)}{\sin^2(\theta_2+\alpha)}\right]. \tag{9}$$

4.3. Pore Water Pressure Power. This work assumes that the volume of the ABE in the failure area does not change; that is, the pore water pressure exerts power on the volume strain is 0, and the power only is done on the boundaries AE and BE. The powers are:

$$W_{u-\text{AE}} = \int_{\theta_2}^{\theta_3} r_1(\theta)\cos\theta\cdot r_u\cdot\gamma\cdot {r_1}^2(\theta)\cdot\omega\cdot\sin\varphi d\theta + \int_{\theta_2}^{\theta_3}(h-r_a\cos\theta_2)\cdot r_u\cdot\gamma\cdot {r_1}^2(\theta)\omega\cdot\sin\varphi d\theta = r_u\cdot\gamma\cdot\omega\cdot {r_a}^2\cdot\sin\varphi[g_4+(h-r_a\cos\theta_2)\cdot g_5], \tag{10}$$

$$W_{u-\text{BE}} = \int_{\theta_1}^{\theta_3}(h+d-r_b\cos\theta_1)\cdot r_u\cdot\gamma\cdot {r_2}^2(\theta)\cdot\omega\cdot\sin\varphi\mathrm{d}\theta + \int_{\theta_1}^{\theta_3} r_2(\theta)\cos\theta\cdot r_u\cdot\gamma\cdot {r_2}^2(\theta)\cdot\omega\cdot\sin\varphi d\theta = r_u\cdot\gamma\cdot\omega\cdot {r_b}^2\cdot\sin\varphi\cdot[(h+d-r_b\cos\theta_1)\cdot g_6+r_b\cdot g_7], \tag{11}$$

where $g_4 \sim g_7$are, respectively:

$$g_4 = \int_{\theta_2}^{\theta_3} e^{[3(\theta-\theta_2)\cdot\tan\varphi]}\cdot\cos\theta\mathrm{d}\theta = \frac{3\tan\varphi\cdot\left(\cos\theta_3\cdot e^{[3(\theta_3-\theta_2)\cdot\tan\varphi]}-\cos\theta_2\right)+\sin\theta_3\cdot e^{[3(\theta_3-\theta_2)\cdot\tan\varphi]}-\sin\theta_2}{1+9\tan^2\varphi}, \tag{12}$$

$$g_5 = \int_{\theta_2}^{\theta_3} e^{[2(\theta-\theta_2)\cdot\tan\varphi]}d\theta = \frac{e^{[2(\theta_3-\theta_2)\cdot\tan\varphi]}-1}{2\tan\varphi}, \tag{13}$$

$$g_6 = \int_{\theta_1}^{\theta_3} e^{[3(\theta_1-\theta)\cdot\tan\varphi]}\cdot\cos\theta d\theta = \frac{3\tan\varphi\cdot\left\{\cos\theta_1-\cos\theta_3\cdot e^{[3(\theta_1-\theta_3)\cdot\tan\varphi]}\right\}+\sin\theta_3\cdot e^{[3(\theta_1-\theta_3)\cdot\tan\varphi]}-\sin\theta_1}{1+9\tan^2\varphi}, \tag{14}$$

$$g_7 = \int_{\theta_1}^{\theta_3} e^{[2(\theta_1-\theta)\cdot\tan\varphi]}d\theta = \frac{1-e^{[2(\theta_1-\theta_3)\cdot\tan\varphi]}}{2\tan\varphi}. \quad (15)$$

In sum, the total power of pore water pressure is:

$$W_u = W_{u\text{–AE}} + W_{u\text{-BE}}. \quad (16)$$

4.4. Internal Energy Dissipation Rate. The internal energy dissipation occurs on the speed discontinuous lines AE and BE, denoted as $W_{V\text{–AE}}$ and $W_{V\text{–BE}}$, respectively. According to formula (2) and geometric relationship, we can get:

$$c = c_0 + \rho(h + r_1\cos\theta - r_a\cos\theta_2), \quad (17)$$

where $W_{V\text{–AE}}$ expression is:

$$\begin{aligned} W_{V\text{-AE}} &= \int_{\theta_2}^{\theta_3} c\cdot(r_1\cdot\omega\cdot\cos\varphi)\cdot\frac{r_1}{\cos\varphi}\mathrm{d}\theta \\ &= \omega\cdot r_a^2\cdot[c_0 + \rho(h - r_a\cos\theta_2)]\cdot g_8 + \omega\cdot\rho\cdot r_a^3\cdot g_9. \end{aligned} \quad (18)$$

$W_{V\text{–BE}}$ expression is:

$$\begin{aligned} W_{V\text{-BE}} &= \int_{\theta_1}^{\theta_3} c\cdot(r_2\cdot\omega\cdot\cos\varphi)\cdot\frac{r_2}{\cos\varphi}d\theta = \omega\cdot r_b^2\cdot[c_0 \\ &\quad + \rho(h - r_a\cos\theta_2)]\cdot g_{10} + \omega\cdot\rho\cdot r_b^3\cdot g_{11}. \end{aligned} \quad (19)$$

The $g_8 \sim g_{11}$ expressions are:

$$g_8 = \frac{e^{[2(\theta_3-\theta_2)\cdot\tan\varphi]} - 1}{2\tan\varphi}, \quad (20)$$

$$\begin{aligned} g_9 &= \int_{\theta_2}^{\theta_3} e^{[3(\theta-\theta_2)\cdot\tan\varphi]}\cdot\cos\theta d\theta \\ &= \frac{3\tan\varphi\cdot\left\{\cos\theta_3\cdot e^{[3(\theta_3-\theta_2)\cdot\tan\varphi]} - \cos\theta_2\right\} + \sin\theta_3\cdot e^{[3(\theta_3-\theta_2)\cdot\tan\varphi]} - \sin\theta_2}{(1+9\tan^2\varphi)}, \end{aligned} \quad (21)$$

$$g_{10} = \frac{1-e^{[2(\theta_1-\theta_3)\cdot\tan\varphi]}}{2\tan\varphi}, \quad (22)$$

$$\begin{aligned} g_{11} &= \int_{\theta_1}^{\theta_3} e^{[3(\theta_1-\theta)\cdot\tan\varphi]}\cdot\cos\theta d\theta \\ &= \frac{3\tan\varphi\cdot\left\{\cos\theta_1 - \cos\theta_3\cdot e^{[3(\theta_1-\theta_3)\cdot\tan\varphi]}\right\} + \sin\theta_3\cdot e^{[3(\theta_1-\theta_3)\cdot\tan\varphi]} - \sin\theta_1}{1+9\tan^2\varphi}. \end{aligned} \quad (23)$$

The dissipation rate of total internal energy is:

$$W_V = W_{V\text{-AE}} + W_{V\text{-BE}}. \quad (24)$$

4.5. Supporting Pressure. Combining the above formulas can derive the analytical expression of the supporting pressure σ_T:

$$\sigma_T = \sigma_a = \frac{2\left(W_\gamma + W_u - W_V\right)}{\omega\cdot r_b^2\cdot\left[1-\sin^2(\theta_1+\alpha)/\sin^2(\theta_2+\alpha)\right]}, \quad (25)$$

$$\text{s.t.}\begin{cases} 0 < \theta_1 < \theta_2 < \pi/2 \\ \theta_2 < \theta_3 < \pi \\ r_a < r_b \end{cases}. \quad (26)$$

Under the constraint condition of formula (26), the minimum value of the supporting pressure in formula (25) can be solved by Matlab software, and it is the best solution. In the final failure condition, the solved supporting pressure is equivalent to the collapse pressure on the shield inclined tunnels excavation face. That is, the failure surface $\sigma_T = \sigma_a$ is the most dangerous failure surface potentially in front of the excavation face.

Table 1: Comparison of results.

α (°)	σ_T (kPa)	Relative error (%)	ρ (kPa/m)	σ_T (kPa)	Relative error (%)	r_u	σ_T (kPa)	Relative error(%)
0	137.0	—	0	142.5	—	0	53.2	—
2	136.6	0.3	0.1	135.8	4.7	0.1	94.5	77.6
4	136.1	0.6	0.2	129.1	9.4	0.2	135.8	155.3
6	135.6	1.0	0.3	122.4	14.1	0.3	177.3	233.3
8	135.5	1.1	0.4	115.7	18.8	0.4	219.1	311.8

5. Result Analysis

5.1. Relative Error. The supporting pressure σ_T on inclined tunnel excavation face is compared with different tunnel inclination angle α, soil heterogeneity coefficient ρ, and pore water pressure coefficient r_u. The parameter results are as follows [30, 31]: the volumetric weight of soil $\gamma = 20\text{kN/m}^3$, tunnel diameter $d = 10$ m, tunnel buried depth $h = 20$ m, initial cohesion $c_0 = 10$ kPa, and internal friction angle $\varphi = 18°$. In Table 1, when the tunnel inclination angle $\alpha = 0°$ and $\alpha = 8°$ ($\rho = 0.1$ kPa/m, $r_u = 0.2$), the supporting pressure σ_T is 137.0 kPa and 135.5 kPa, respectively, and the relative error is 1.1%. When the soil heterogeneity coefficient $\rho = 0$ and $\rho = 0.4$ kPa/m ($\alpha = 5°$, $r_u = 0.2$), the supporting pressure σ_T is 142.5 kPa and 115.7 kPa, respectively, and the relative error is 18.8%. When the pore water pressure coefficient $r_u = 0$ and $r_u = 0.4$ ($\alpha = 5°$, $\rho = 0.1$ kPa/m), the supporting pressure σ_T is 53.2 kPa and 219.1 kPa, respectively, and the relative error is 311.8%. They have different degrees of influences on the supporting pressure of excavation face. The coefficient of pore water pressure r_u has a foremost effect and then is the coefficient of soil heterogeneity ρ, and the influence of the inclination angle α is relatively small.

5.2. Supporting Pressure Analysis. The influence of soil heterogeneity and pore water pressure on the supporting pressure of the excavation face is investigated, where tunnel

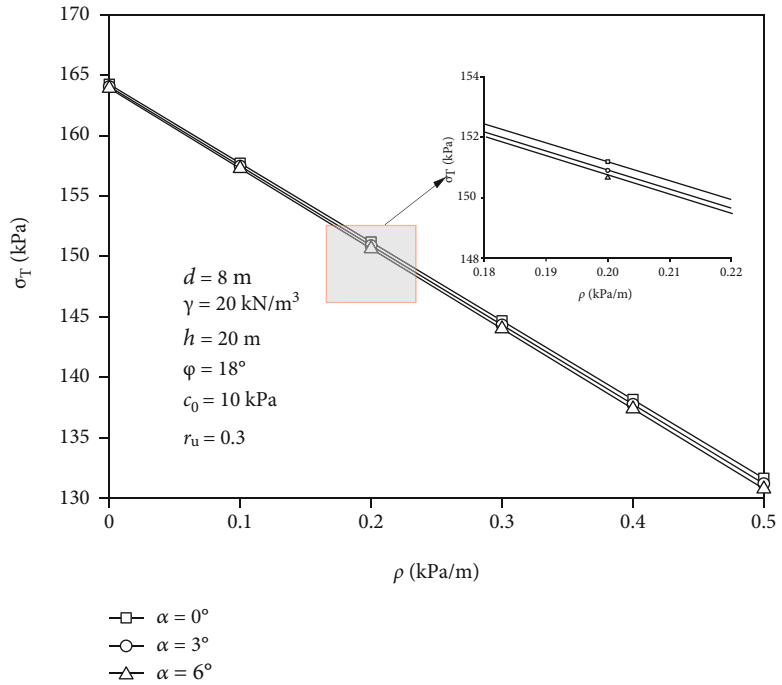

(a)

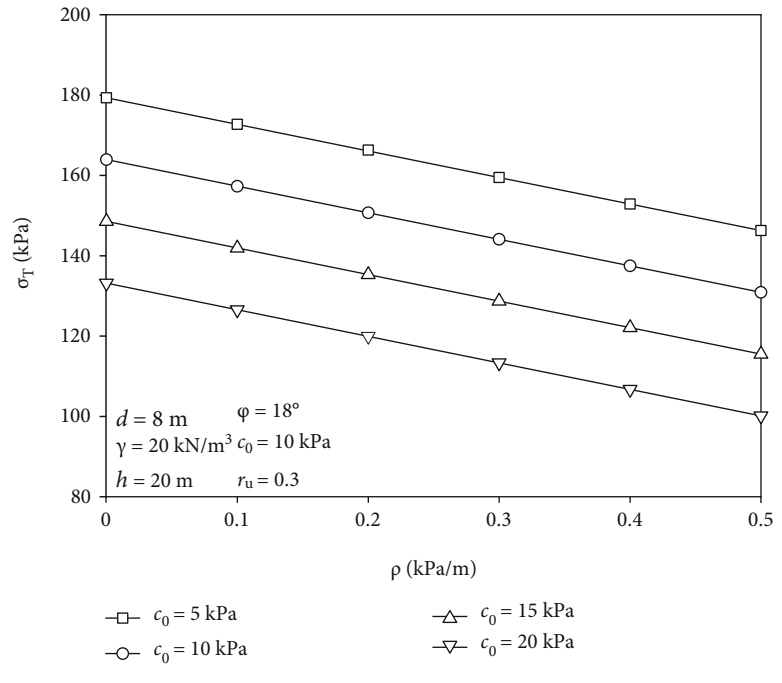

(b)

Figure 2: Continued.

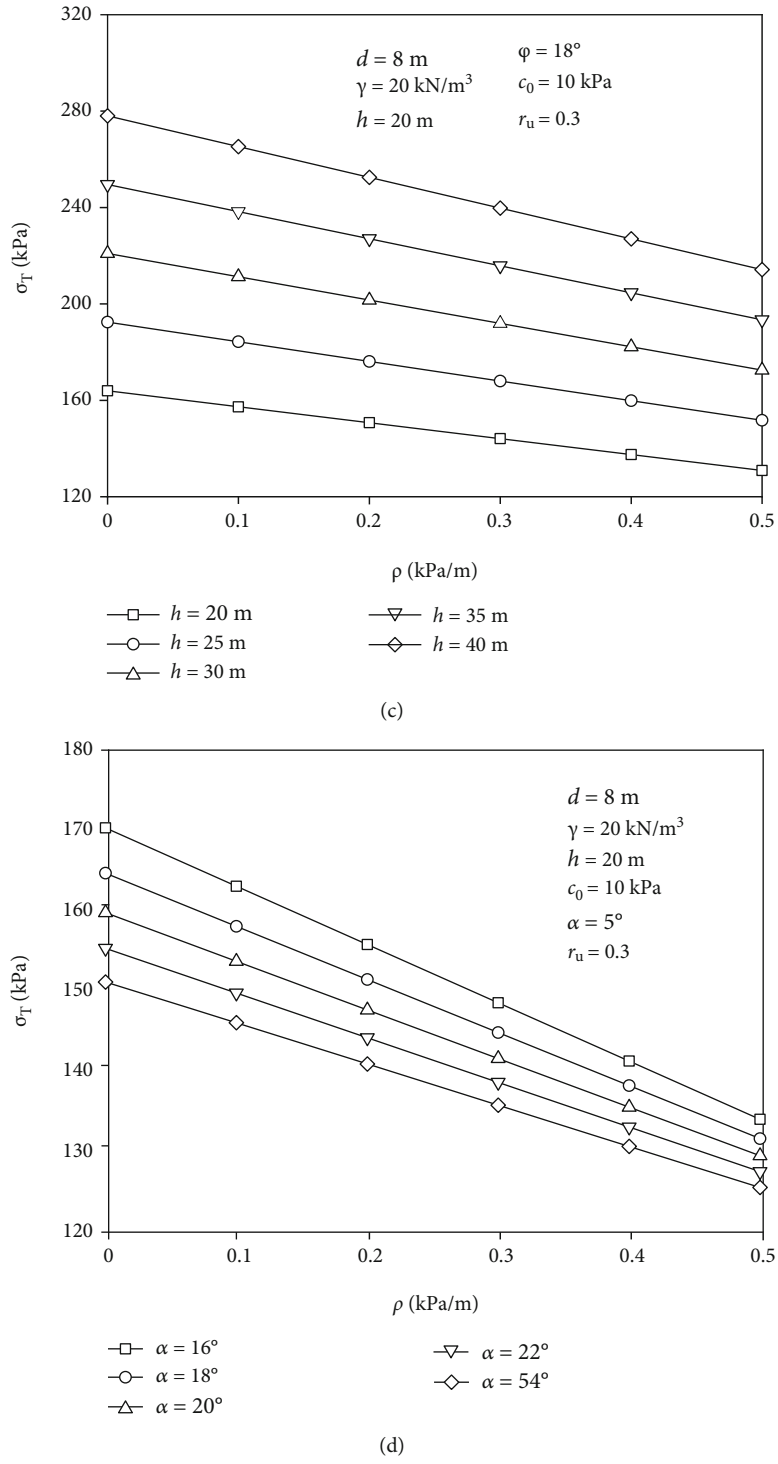

Figure 2: Influence of soil heterogeneity on the supporting pressure: (a) tunnel inclination angle α; (b) initial cohesion c_0; (c) buried depth h; and (d) internal friction angle φ.

diameter $d = 8\,m$, tunnel buried depth $h = 20\,m \sim 40\,m$, the volumetric weight of soil $\gamma = 20\text{kN/m}^3$, initial cohesion $c_0 = 5\,\text{kPa} \sim 25\,\text{kPa}$, internal friction angle $\varphi = 16^\circ \sim 24^\circ$,the tunnel inclination angle $\alpha = 0^\circ \sim 6^\circ$, the soil heterogeneity coefficient $\rho = 0\,\text{kPa/m} \sim 0.5\,\text{kPa/m}$, and the pore water pressure coefficient $r_u = 0 \sim 0.4$.

5.2.1. Influence of Soil Heterogeneity. Figure 2 reflects the effect of soil heterogeneity on the supporting pressure of excavation face. Overall, as the soil heterogeneity coefficient ρ increases, the supporting pressure σ_T gradually decreases. Because while the buried depth remains constantly, the increase of the soil heterogeneity coefficient ρ causes the

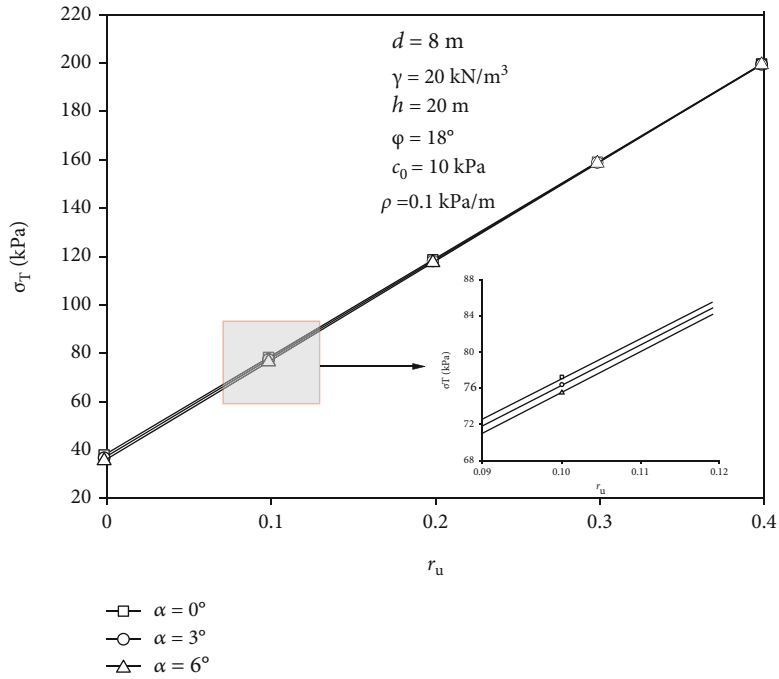

(a)

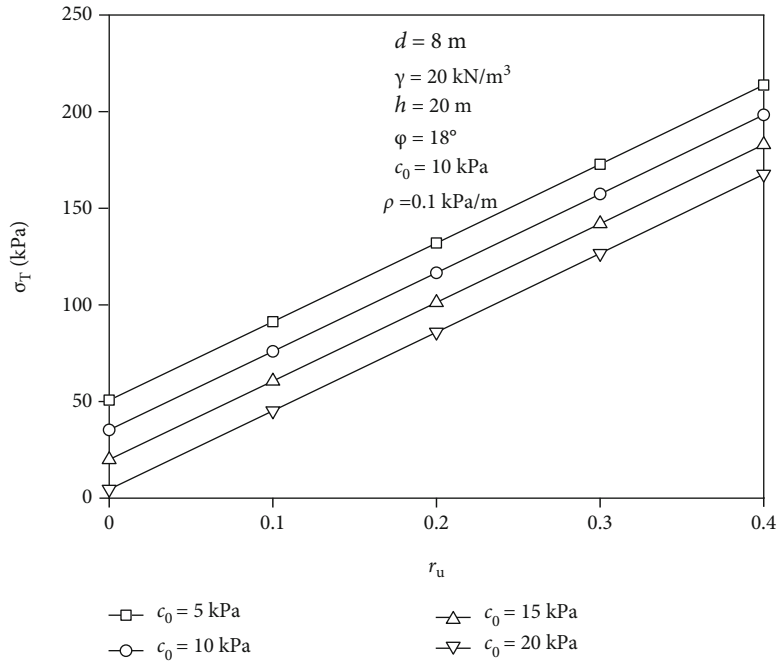

(b)

Figure 3: Continued.

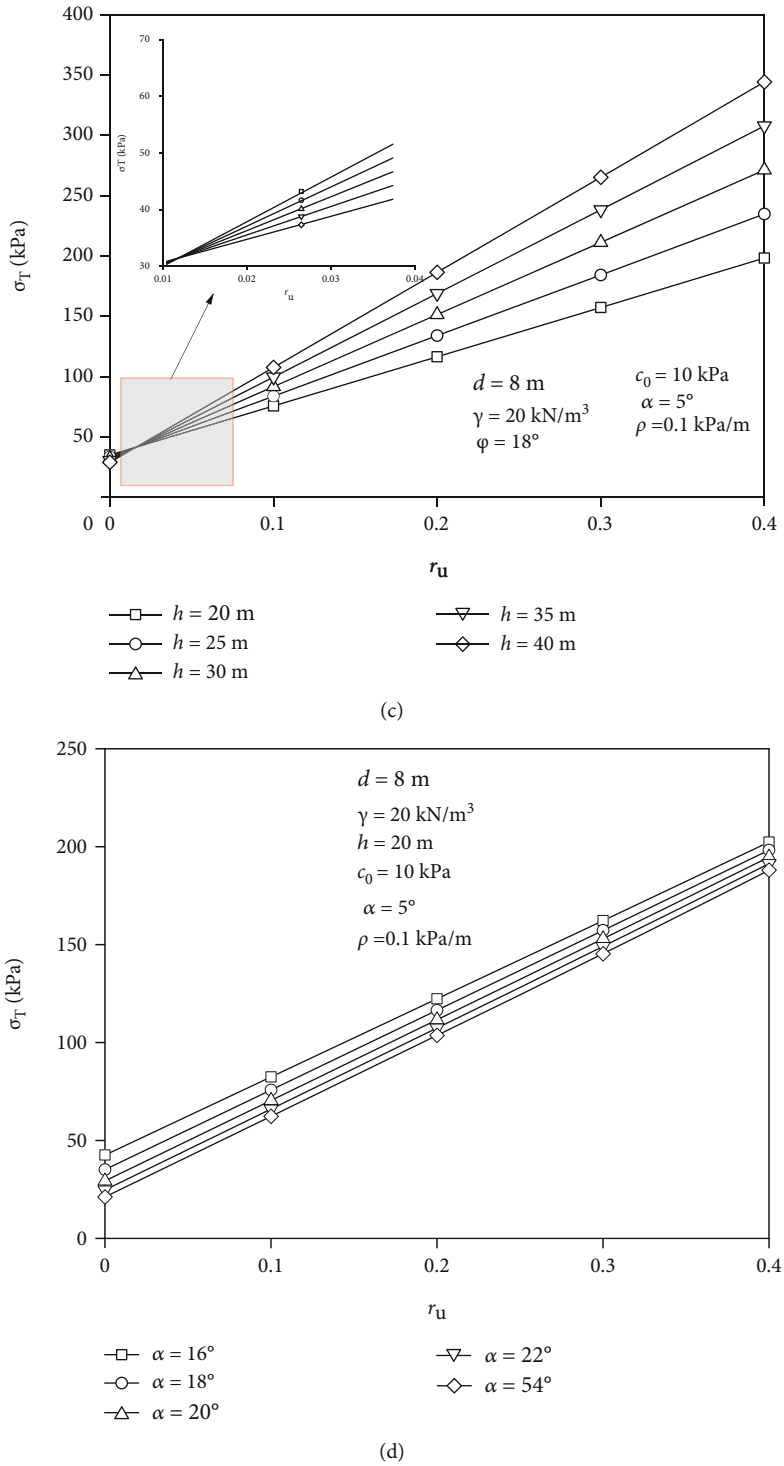

Figure 3: Influence of pore water pressure on the supporting pressure: (a) tunnel inclination angle α; (b) buried depth h; (c) initial cohesion c_0; and (d) internal friction angle φ.

increase of soil cohesion, and the stability of soil is increased accordingly.

In Figure 2(a), the three curves are very close and almost coincide. When the soil heterogeneity coefficient $\rho = 0.5$ kPa/m, the tunnel inclination angle α is 0°, 3°, and 6°, and the supporting pressures corresponding to 131.6 kPa, 131.2 kPa, 130.8 kPa, and the error is 0.4 kPa and 0.4 kPa, respectively. It indicates that a small adjustment in the tunnel inclination angle α has a relatively limited influence on the excavation face support. In Figure 2(b), the supporting pressure σ_T displays a diminishing trend as the initial cohesive c_0 increases. When the soil heterogeneity coefficient ρ

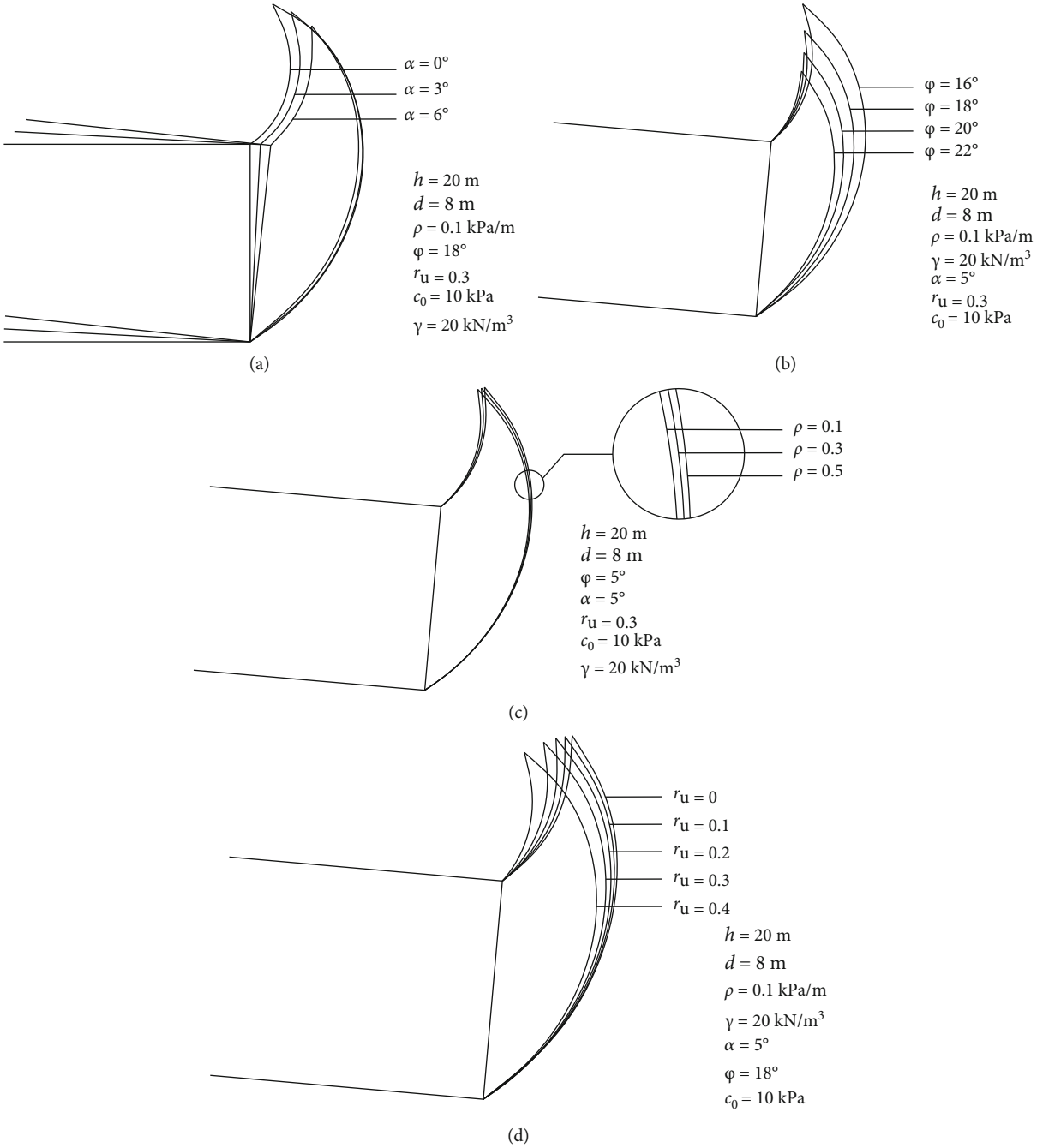

Figure 4: Influence of parameters on the position of failure surface: (a) tunnel inclination angle α; (b) internal friction angle φ; (c) coefficient of soil heterogeneity ρ; and (d) pore water pressure coefficient r_u.

= 0.5 kPa/m, the initial cohesion c_0 increases from 5 kPa to 20 kPa, and the relative error is 31.6%. It indicates that the initial cohesive has a greater effect on the supporting pressure on the inclined tunnel excavation face. The initial cohesive be greater, the supporting pressure that must be supplied to the excavation face be smaller. In Figure 2(c), as the buried depth h gradually increases, the excavation face supporting pressure σ_T increases accordingly. When the soil heterogeneity coefficient $\rho = 0.3$ kPa/m, the buried depth h increases from 20 m to 40 m, and the supporting pressure σ_T increases from 144.1 kPa to 239.8 kPa, a growth rate of 66.4%. This reflects how pore water pressure affects supporting pressure. As buried depth h increases, the cohesive and pore water pressure of the soil increases. While the cohesive increases, the supporting pressure should decrease (see Figure 2(b)), but the supporting pressure increases. It shows that pore water pressure has an obvious increase impact on support pressure. In Figure 2(d), when the soil heterogeneity coefficient is not considered ($\rho = 0$), the internal friction angle $\varphi = 16^\circ$ increases to $\varphi = 24^\circ$, the supporting pressure

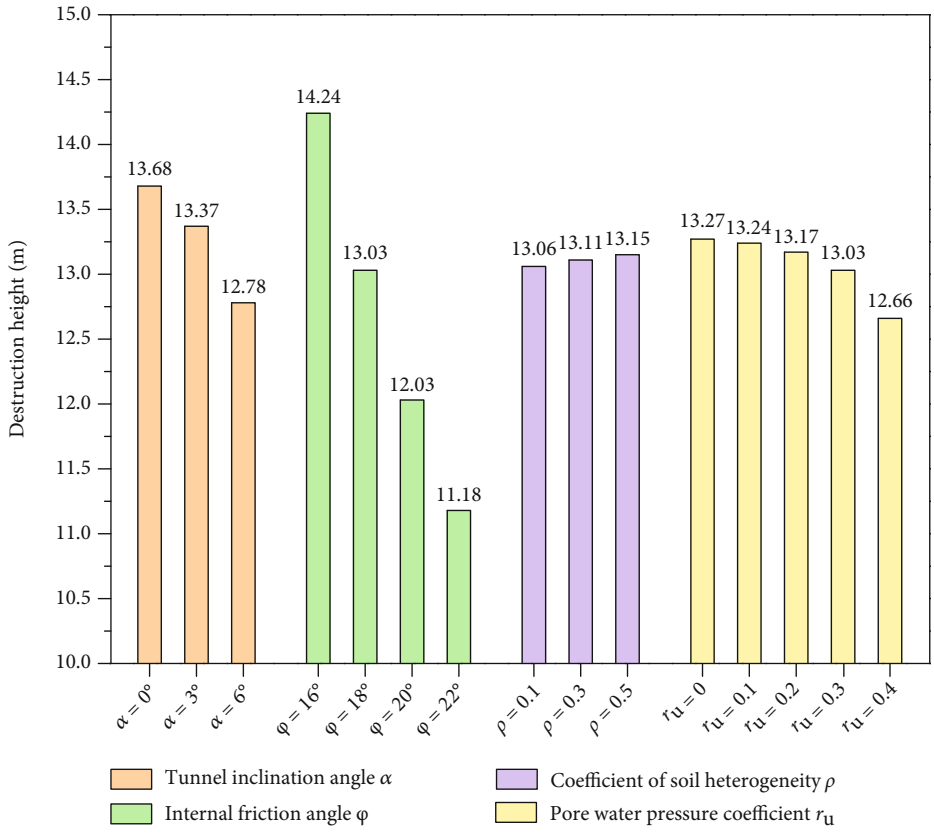

Figure 5: The influence of parameters on the height of the failure surface.

decreases from 169.6 kPa to 150.4 kPa, and the relative error is 11.3%. When considering the soil heterogeneity coefficient ($\rho = 0.5$ kPa/m), the internal friction angle $\varphi = 16^{\circ}$ increases to $\varphi = 24^{\circ}$, while the supporting pressure decreases from 133.3 kPa to 124.8 kPa, and the relative error is 6.4%. It indicates that the increase of the friction angle φ in the soil has a reduced effect on supporting pressure, which is mainly manifested when the soil heterogeneity is weak.

5.2.2. Pore Water Pressure Impact. In Figure 3 as the pore water pressure coefficient r_u gradually increases, the supporting pressure σ_T tends to increase. It indicates that pore water has a considerable impact on the supporting pressure required for the inclined tunnel excavation face. To guarantee the excavated face stability, the supporting pressure on excavation face must be strengthened.

Figure 3(a) shows that several curves almost overlap. It shows that under the action of pore water, the tunnel inclination α has a limited influence on the supporting pressure σ_T. In Figure 3(b), the supporting pressure σ_T decreases with the increase of the initial cohesive c_0. When initial cohesive c_0 increases from 5 kPa to 20 kPa ($r_u = 0.4$), the supporting pressure σ_T relative error is 21.6%, and the initial cohesion c_0 influences the supporting pressure σ_T significantly. In Figure 3(c), when the pore water pressure coefficient r_u is small, as the buried depth h increases, the supporting pressure σ_T gradually decreases. While the pore water pressure coefficient r_u increases in time, the supporting pressure σ_T increases in tandem with the buried depth h. Because as buried depth h increases, the soil heterogeneity causes the increase in the cohesive c to reduce the supporting pressure σ_T, while the pore water pressure increases caused the supporting pressure σ_T increases. Following these, when the pore water pressure coefficient r_u is between 0.01 and 0.02, the effect of the heterogeneity coefficient and the pore water pressure coefficient on the support pressure is similar. When the pore water pressure coefficient r_u is less than 0.01, the effect of soil heterogeneity on the reduction of the support pressure is dominant, while as the pore water pressure coefficient r_u increases to greater than 0.02, the pore water pressure on the support pressure increases gradually and becomes dominant. When considering pore water pressure coefficient ($r_u = 0.4$), the internal friction angle φ increases from 16° to 24°, and the corresponding supporting pressure σ_T decreases from 202.4 kPa to 188.0 kPa, with a relative error of 7.1%. It demonstrates that the smaller the pore water pressure coefficient, the more obvious the reduction effect of the soil friction angle φ on the supporting pressure.

5.2.3. Failure Surface. Figures 4 and 5 depicts the influence of related parameters on the inclined tunnel failure surface. In Figure 4(a), as the tunnel inclination α increases, the failure surface moves in the direction of excavation and the failure height decreases. In Figure 4(b), as the internal friction angle φ increases, the failure range diminishes, the location of the failure surface approaches the hole, and the failure height

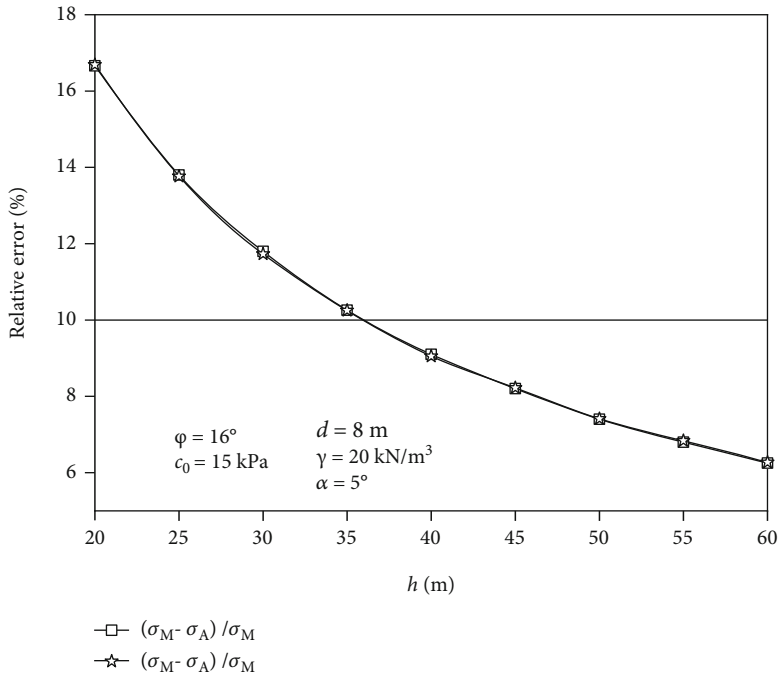

(a)

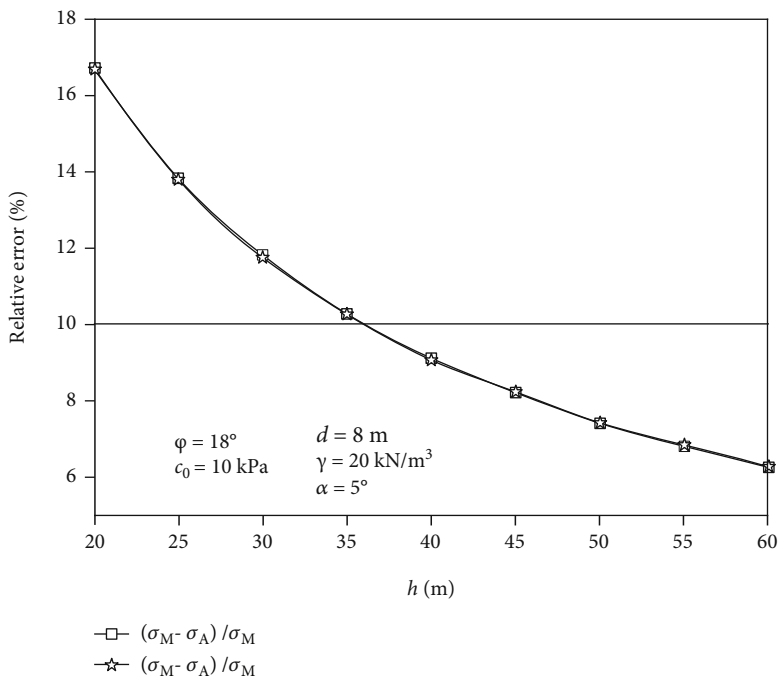

(b)

Figure 6: Continued.

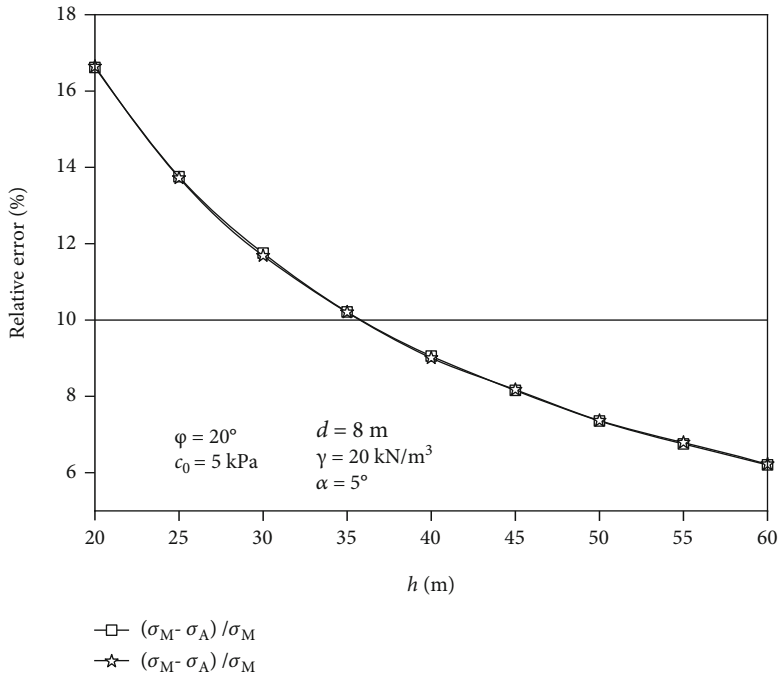

(c)

Figure 6: Variation laws of the relative error of different parts supporting pressure: (a) $\varphi = 16^\circ$, $c = 15$ kPa; (b) $\varphi = 18^\circ$, $c = 10$ kPa; and (c) $\varphi = 20^\circ$, $c = 5$ kPa.

Table 2: Boundary depth of shallow tunnels under the influence of soil heterogeneity and pore water.

	Allowable error Δ		
	10%	8%	6%
$\varphi = 16^\circ$, $c_0 = 15$ kPa	25 m ~ 30 m	35 m ~ 40 m	55 m ~ 60 m
$\varphi = 18^\circ$, $c_0 = 10$ kPa	25 m ~ 30 m	35 m ~ 40 m	50 m ~ 55 m
$\varphi = 20^\circ$, $c_0 = 5$ kPa	20 m ~25 m	35 m ~ 40 m	50 m ~ 55 m

decreases. In Figure 4(c), as the soil heterogeneity coefficient ρ increases, the failure range does not change much, the location of the failure surface develops toward the excavation direction, and the failure height decreases slightly. In Figure 4(d), as the pore water pressure coefficient r_u increases, the failure range decreases, the location of the failure surface gradually approaches the cave, and the failure height decreases. It can be shown that the internal friction angle φ, tunnel inclination angle α, and pore water pressure coefficient r_u have greater effect on the failure surface except the soil heterogeneity coefficient ρ.

5.2.4. Supporting Pressure at the Top, Middle, and Bottom of the Excavation Face in the Shallow Buried Section. The above results assume that the inclined tunnel is in the deep buried section, and the supporting pressure applied at the top, middle, and bottom of the excavation face is in a uniformly distributed form, that is, $\sigma_A = \sigma_M = \sigma_B$. However, the supporting pressure of the three parts in the shallow buried section is different, so the division of the boundary between deep buried and shallow buried is particularly important.

Assuming that the surrounding rock grade is VI, the diameter of the inclined tunnel is $d = 8$ m, and the shallow tunnel boundary $H_P = 37.4$ m ~ 46.8 m is calculated via the "Code for Design of Railway Tunnels" (TB 10003-2016) [31]. Regardless of soil heterogeneity and pore water influence ($\rho = 0$ and $r_u = 0$), using the method in the work, the relative error of three parts of the inclined tunnel excavation face can be obtained as a rule of the buried depth h. In Figure 6, the relative error between the three supporting pressures shows a decreasing trend as the buried depth h increases. If the relative error of $\Delta = 10\%$ is regarded as no difference, that is, three supporting pressures are equal, then, the shallow tunnel boundary $H_P = 35$ m ~ 40 m can be obtained. Therefore, the results of this work are in good accord with the normative results, which confirms the validity of the results of this work.

On the basis of the above research, considering the soil heterogeneity and the influence of pore water ($\rho = 0.1$ kPa/m and $r_u = 0.3$), the shallow tunnel boundary is obtained, as shown in Table 2. If the relative error of the supporting pressure is $\Delta = 10\%$ is the allowable error, then, the shallow tunnel boundary $H_P = 20$ m ~ 30 m. While it does not consider the soil heterogeneity and pore water ($\rho = 0$ and $r_u = 0$), the shallow tunnel boundary change is -15 m ~ -10 m. Depending on $\Delta = 8\%$as the allowable error, then, the boundary of the shallow tunnel $H_P = 35$ m ~ 40 m , contrast $\Delta = 10\%$, and the limit of the shallow tunnel changes 10 m ~ 15 m. Depending on $\Delta = 6\%$ is the allowable error, then the boundary of shallow tunnel $H_P = 50$ m ~ 60 m, and contrast $\Delta = 8\%$, the boundary change of the shallow

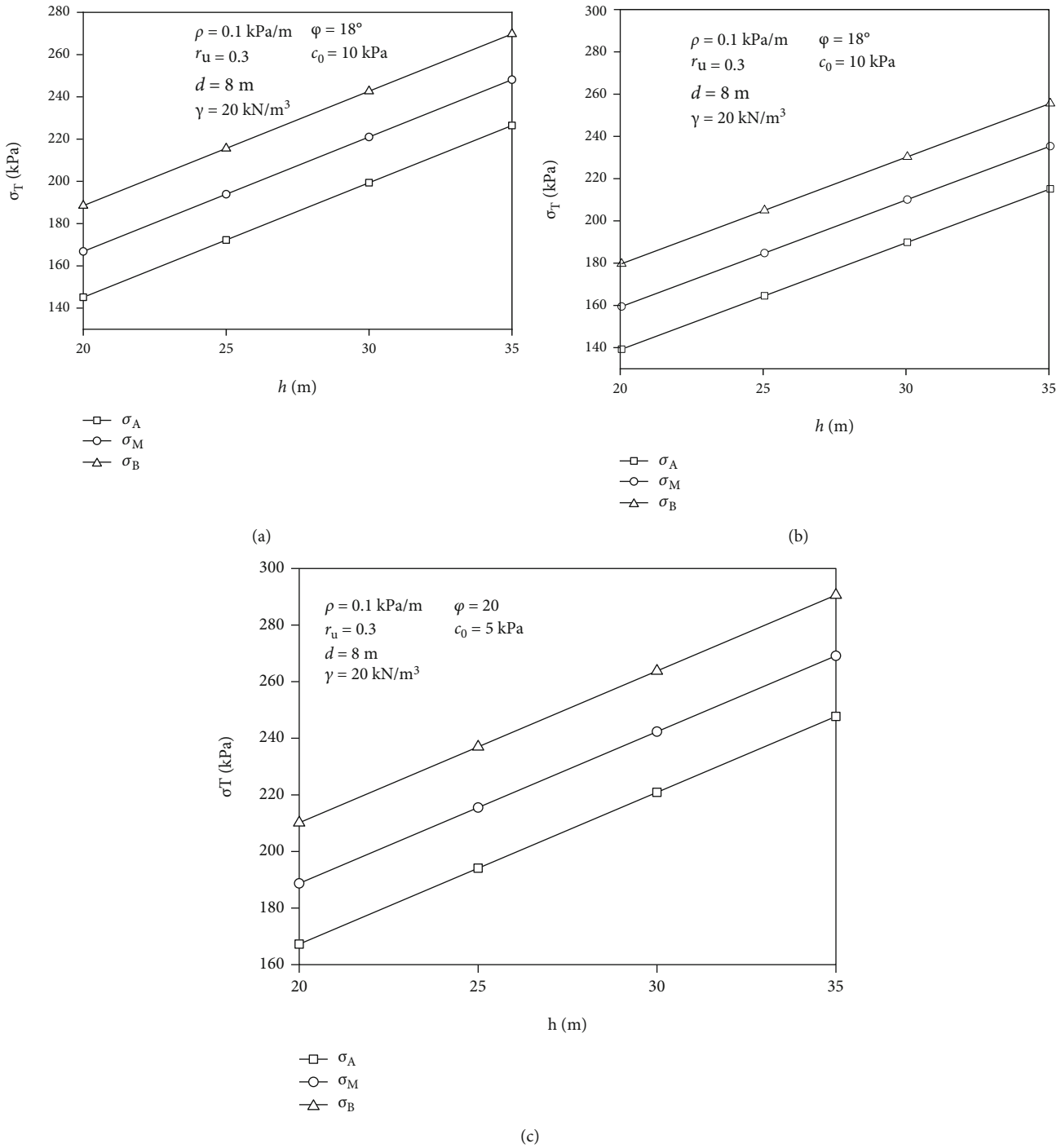

Figure 7: Change rules of different parts supporting pressure with the buried depth h considering the effect of soil heterogeneity and pore water: (a) $\varphi = 16^{\circ}$, $c_0 = 15$ kPa; (b) $\varphi = 18^{\circ}$, $c_0 = 10$ kPa; and (c) $\varphi = 20^{\circ}$, $c_0 = 5$ kPa.

Table 3: Stratum parameters.

Soil layer	Unit weight/(kN/m^3)	Cohesion/kPa	Internal friction angle/(°)	Layer thickness/m
①Artificial fill	17.3	12	28	1.4
②Silty soil	18.5	6.0	18	7.6
③Alluvial strata	19.5	0.8	18	6.0
④Strongly weathered mudstone	21.6	200	24	23.0

Table 4: Comparison of results.

Monitoring value [32]		This work	
Minimum value/kPa	Maximum value/kPa	Minimum value/kPa	Maximum value/kPa
38	174	37.6	161.9

tunnel is 15 m ~ 20 m. It can be seen that soil heterogeneity and pore water pressure have a substantial effect on the boundary of shallow tunnels, and the results of this work supplement the specification.

In addition, the supporting pressure that needs to be applied to the top, middle, and bottom of the shallow tunnel excavation face is given. In Figure 7, as the buried depth h increases, the supporting pressure σ_T of the three parts also increases accordingly, and the required supporting pressure at the bottom is the largest, followed by the middle, and the smallest at the top, that is, $\sigma_B > \sigma_M > \sigma_A$. It indicates that in the shallow buried section, the supporting pressure required from the top to the bottom of the inclined tunnel excavation face gradually increases. It is suggested that the required supporting pressure on three different parts should be reasonably applied in the actual process to prevent the tunneling direction from deviating from the design axis.

6. Application of Results

A collapse accident occurred on line 3 of a subway. The diameter of the shield tunnel is $d = 6.0$ m, the buried depth is $h = 12$ m, and the tunnel inclination angle is $\alpha = 0$. The strata that the tunnel passes through are mainly alluvial layers and strongly weathered mudstone. The physical and mechanical properties of the soil layers in this area are shown in Table 3 after site survey. After conversion, the unit weight of rock and soil masses is $\gamma = 19.3\text{kN/m}^3$, internal friction angle is $\varphi = 19.8^\circ$, initial cohesion of soil is $c_0 = 12$ kPa, heterogeneity coefficient is $\rho = -0.65$ kPa/m, and pore water pressure coefficient is $r_u = 0.51$. The surrounding rock pressure was solved via this method, and it was compared with the existing result and on-site measured result as shown in Table 4. In Table 4, the minimum value from this work is 37.6 kPa, without considering the effect of pore water pressure. The minimum field monitoring value (as no pore water situation) is 38 kPa, with a relative error of 1%. Similarly, when considering the groundwater, the maximum value is 161.9 kPa and 174 kPa, respectively, and the relative error is 7.0%. The above shows that the result from this work is in good agreement with the actual monitoring value, which verifies the applicability of this method.

7. Conclusions

(1) There are two effects in the tunneling process of shield inclined tunnels. One is as the buried depth increases, the soil heterogeneity enhances the cohesive which reduces the supporting pressure. Another is that the increase of the buried depth also causes the pore water pressure to intensify, leading to an augmenting effect on the supporting pressure. Following these when the buried depth is small, the effect of soil heterogeneity on the reduction of the supporting pressure dominates. However, when the buried depth gradually increases, the augmenting effect of pore water pressure on the supporting pressure gradually dominates

(2) Soil heterogeneity, initial cohesion, and soil heterogeneity coefficient have substantial influence on the required supporting pressure on the excavation face. But it has little effect on the position of the potential failure surface in front of the excavation. Compared the initial cohesion $c_0 = 5$ kPa and 20 kPa ($\rho = 0.5$ kPa/m), the relative error of the supporting pressure can reach 31.6%. The pore water pressure and the soil friction angle have a significant effect on the required supporting pressure on the excavation face. And as the pore water pressure and the soil friction angle increase, the potential failure surfaces are all approach to the cave, and the failure range gradually decreases. Compared the pore water pressure coefficient $r_u = 0$ and 0.4 ($\varphi = 18^\circ$), the relative error of the supporting pressure can reach 464.1%. Comparing the internal friction angle $\varphi = 16^\circ$ and 24° ($r_u = 0$), the relative error of the supporting pressure can reach 50.4%. In addition, the small increase of the tunnel inclination has little effect on the required supporting pressure on the excavation face. But, the location of its potential failure surface expands in the direction of excavation

(3) Without considering the influence of soil heterogeneity and pore water ($\rho = 0$ and $r_u = 0$), the shallow tunnel boundary $H_P = 37.4$ m ~ 46.8 m is calculated according to the specification. The shallow tunnel boundary $H_P = 35$ m ~ 40 m under the condition of allowable error $\Delta = 10\%$ is obtained by the method in this work. The results of this work are similarity to the normative results, which verifies the validity of the results of this work. In addition, considering the soil heterogeneity and the influence of pore water ($\rho = 0.1$ kPa/m and $r_u = 0.3$), according to the allowable error $\Delta = 10\%$, 8%, and 6%, the boundary of the shallow tunnel is $H_P = 20$ m ~ 30 m, 35 m ~ 40 m, and 50 m ~ 60 m, respectively. It can be seen that the soil heterogeneity and the pore water effect significantly affect the boundary of the shallow tunnel

Data Availability

The data used to support the findings of this study are available from the corresponding author upon request.

Conflicts of Interest

All authors declare that they have no conflict of interest or financial conflicts to disclose.

Acknowledgments

The work is supported by the National Natural Science Foundation of China (52074116 and 51804113).

References

[1] Q. H. Wu, L. Weng, Y. L. Zhao, and F. Feng, "Influence of infilling stiffness on mechanical and fracturing responses of hollow cylindrical sandstone under uniaxial compression tests[J]," *Journal of Central South University*, vol. 28, no. 8, pp. 2485–2498, 2021.

[2] L. Weng, Q. H. Wu, Y. L. Zhao, and S. M. Wang, "Dynamic response and failure of rock in initial gradient stress field under stress wave loading[J]," *Journal of Central South University*, vol. 27, no. 3, pp. 963–972, 2020.

[3] D. B. Zhang and B. Zhang, "Stability analysis of the pressurized 3D tunnel face in anisotropic and nonhomogeneous soils[J]," *International Journal of Geomechanics*, vol. 20, no. 4, pp. 1–18, 2020.

[4] X. Y. Hu, Z. X. Zhang, and S. Kieffer, "A real-life stability model for a large shield-driven tunnel in heterogeneous soft soils[J]," *Frontiers of Structural and Civil Engineering*, vol. 6, no. 2, pp. 176–187, 2012.

[5] A. Bobet, "Effect of pore water pressure on tunnel support during static and seismic loading," *Tunnelling and Underground Space Technology*, vol. 18, no. 4, pp. 377–393, 2003.

[6] B. Zhang, Z. Y. Ma, X. Wang, J. S. Zhang, and W. Q. Peng, "Reliability analysis of anti-seismic stability of 3D pressurized tunnel faces by response surfaces method," *Geomechanics and Engineering*, vol. 20, no. 1, pp. 43–54, 2020.

[7] D. B. Zhang, W. C. Sun, C. Y. Wang, and B. Yu, "Reliability analysis of seismic stability of shield tunnel face under multiple correlated failure modes[J]," *KSCE Journal of Civil Engineering*, vol. 25, no. 8, pp. 3172–3185, 2021.

[8] Q. J. Pan and D. Dias, "Face stability analysis for a shield-driven tunnel in anisotropic and nonhomogeneous soils by the kinematical approach[J]," *International Journal of Geomechanics*, vol. 16, no. 3, p. 04015076, 2016.

[9] G. Mollon, D. Daniei, and A. H. Soubra, "Rotational failure mechanisms for the face stability analysis of tunnels driven by a pressurized shield," *International Journal for Numerical and Analytical Methods in Geomechanics*, vol. 35, no. 12, pp. 1363–1388, 2011.

[10] B. Zhang, Y. Jiang, H. Cheng, and Z. Liu, "Upper bound analysis of the stability of 3D slopes in the saturated soft clay subjected to seismic effect[J]," *Frontiers in Earth Science*, vol. 9, p. 795854, 2021.

[11] B. Zhang, J. Jiang, D. B. Zhang, and Z. Liu, "Upper bound solution of collapse pressure and permanent displacement of 3D tunnel faces using the pseudo-dynamic method and the kinematic approach," *Geomechanics and Engineering*, vol. 25, no. 6, pp. 521–533, 2021.

[12] M. S. Huang, S. Li, J. Yu, and J. Q. W. Tan, "Continuous field based upper bound analysis for three-dimensional tunnel face stability in undrained clay," *Computers and Geotechnics*, vol. 94, pp. 207–213, 2018.

[13] J. H. Zhang, W. J. Wang, D. B. Zhang, B. Zhang, and F. Meng, "Safe range of retaining pressure for three-dimensional face of pressurized tunnels based on limit analysis and reliability method[J]," *KSCE Journal of Civil Engineering*, vol. 22, no. 11, pp. 4645–4656, 2018.

[14] H. Z. Cheng, J. Chen, R. P. Chen, and G. L. Chen, "Reliability study on shield tunnel face using a random limit analysis method in multilayered soils," *Tunnelling and Underground Space Technology*, vol. 84, pp. 353–363, 2019.

[15] E. Ibrahim, A. H. Soubra, G. Mollon, W. Raphael, D. Dias, and A. Reda, "Three-dimensional face stability analysis of pressurized tunnels driven in a multilayered purely frictional medium," *Tunnelling and Underground Space Technology*, vol. 49, no. 1, pp. 18–34, 2015.

[16] K. H. Han, C. P. Zhang, and D. L. Zhang, "Upper-bound solutions for the face stability of a shield tunnel in multilayered cohesive-frictional soils," *Computers and Geotechnics*, vol. 79, pp. 1–9, 2016.

[17] Q. J. Pan and D. Dias, "Upper-bound analysis on the face stability of a non-circular tunnel," *Tunnelling and Underground Space Technology*, vol. 62, pp. 96–102, 2017.

[18] S. Senent, C. Yi, and R. Jimenez, "An upper bound solution for tunnel face stability analysis considering the free span," *Tunnelling and Underground Space Technology*, vol. 103, p. 103515, 2020.

[19] G. H. Chen, J. F. Zou, and J. Q. Chen, "Shallow tunnel face stability considering pore water pressure in non- homogeneous and anisotropic soils," *Computers and Geotechnics*, vol. 116, p. 103205, 2019.

[20] Y. Li, C. Lyu, M. N. Wang, and T. Y. Xu, "Three-dimensional upper bound limit analysis of a deep soil-tunnel subjected to pore pressure based on the nonlinear Mohr-Coulomb criterion," *Computers and Geotechnics*, vol. 112, pp. 293–301, 2019.

[21] J. S. Xu, D. C. Du, and Z. H. Yang, "Upper bound analysis for deep tunnel face with joined failure mechanism of translation and rotation[J]," *Journal of Central South University*, vol. 22, no. 11, pp. 4310–4317, 2015.

[22] J. H. Zhang, W. J. Wang, B. Zhang, and D. B. Zhang, "Upper bound analysis for collapse failure of shield tunnel face excavated in unsaturated soils considering steady vertical flow," *Mathematical Problems in Engineering*, vol. 2019, 10 pages, 2019.

[23] F. Huang and X. L. Yang, "Upper bound limit analysis of collapse shape for circular tunnel subjected to pore pressure based on the Hoek-Brown failure criterion," *Tunnelling and Underground Space Technology incorporating Trenchless Technology Research*, vol. 26, no. 5, pp. 614–618, 2011.

[24] Q. J. Pan and D. Dias, "The effect of pore water pressure on tunnel face stability," *International Journal for Numerical and Analytical Methods in Geomechanics*, vol. 40, no. 15, pp. 2123–2136, 2016.

[25] D. B. Zhang, Z. Y. Ma, B. Yu, and H. D. Yin, "Upper bound solution of surrounding rock pressure of shallow tunnel under nonlinear failure criterion[J]," *Journal of Central South University*, vol. 26, no. 7, pp. 1696–1705, 2019.

[26] Z. W. Li, X. L. Yang, and T. Z. Li, "Face stability analysis of tunnels under steady unsaturated seepage conditions," *Tunnelling and Underground Space Technology*, vol. 93, p. 103095, 2019.

[27] J. H. Zhang and B. Zhang, "Reliability analysis for seismic stability of tunnel faces in soft rock masses based on a 3D stochastic collapse model [J]," *Journal of Central South University*, vol. 26, no. 7, pp. 1706–1718, 2019.

[28] J. H. Zhang, L. Y. Zhang, W. J. Whang, D. B. Zhang, and B. Zhang, "Probabilistic analysis of three-dimensional tunnel face stability in soft rock masses using Hoek–Brown failure

criterion," *International Journal for Numerical and Analytical Methods in Geomechanics*, vol. 44, no. 11, pp. 1601–1616, 2020.

[29] W. F. Chen, *Limit analysis and soil plasticity*, J. Ross Publishing, Inc, Florida, 2007.

[30] Q. Liang, X. L. Yang, J. H. Zhang, and W. Q. Zhou, "Upper bound analysis for supporting pressure of shield tunnel in heterogeneous soil," *Rock and Soil Mechanics*, vol. 37, no. 9, pp. 2585–2592, 2016.

[31] National Railway Administration of the People's Republic China, "TB 10003-2016, Code for Design of Rai1way Tunnel," in China Railway Publishing House Co., Ltd, 2016.

[32] J. L. Qiao, *Analysis of shield tunnel face stability*, Tianjin University, Tianjin, 2008.